Heliyon 8 (2022) e08743

Contents lists available at ScienceDirect

Heliyon

journal homepage: www.cell.com/heliyon

Research article

UV-irradiated sol-gel spin coated AZO thin films: enhanced optoelectronic properties

Md. Irfan Khan, Tasratur Reaj Neha, Md. Muktadir Billah *

Department of Materials and Metallurgical Engineering, Bangladesh University of Engineering and Technology, Dhaka, 1000, Bangladesh

ARTICLE INFO

Keywords:
Thin film
Sol-gel
Optoelectronic
Burstein-moss effect
UV irradiation
UV blocking

ABSTRACT

Thin films of transparent conductive Al doped ZnO (AZO) thin films were produced via sol-gel spin coating route. Structural, optical, and electrical properties were explored for several dopant concentrations. Formation of crystalline AZO was verified by X-ray Diffraction (XRD) Analysis and structural analysis were carried out later from the XRD data. Highest band gap of 3.67 eV was found for 2 mol % AZO thin films. The average transmittance was found to be 84.19% in the visible spectra for the corresponding thin films. 2 mol% AZO also exhibited a minimum resistivity of 2.05 Ω-cm with a maximum value of figure of merit. Prolonged UV irradiation was applied to 2 mol % AZO thin films prior to annealing. It significantly modified the surface morphology of the film and provided shielding near UVA (315–378 nm) spectrum. This also enhanced the conductivity of the thin film by 3-fold compared to non-UV treated sample and decreased optical band gap significantly.

1. Introduction

Doped ZnO thin films have grabbed immense attention as transparent conductive oxide (TCO) for empirical applications in electroluminescent devices and solar cells [1, 2, 3, 4, 5]. ZnO exhibits anisotropic crystalline structure oriented along (002) plane having a direct bandgap about 3.37 eV [6, 7]. Owing low cost, availability, non-toxicity and excellent opto-electronic properties, ZnO thin film would be a good substitute to the extensively utilized indium tin oxide (ITO) thin film [8]. High valence impurities such as Al, Ga, In etc. can further enhance the conductivity of ZnO up to about 10^{-4} S/cm by donor electrons [9, 10]. Such thin films are widely prepared using sol-gel route because of versatile compositional control, affordable cost, homogeneity in molecular level for mixing of liquid precursors and lower crystallization temperature [11]. In alkoxide route, organo-metallic precursors are expensive and sometimes hazardous. Therefore non-alkoxide route is more preferable. ZnO thin film prepared using different types of precursors, solvents and stabilizers are reported in literature to tailor its structural and opto-electronic properties. However, when as solvents 2-methoxy ethanol and as stabilizer mono-ethanolamine (MEA) were used, this results in high c-axis orientation [12, 13]. Many experiments on doped ZnO thin films made by sol-gel processing have been published. However, there remains some difficulties associated with the aqueous sol–gel method, as hydrolysis, condensation, and dry out take place concurrently, resulting in difficulty in reproducing the final product and tailoring target properties.

Apart from that, band gap of ZnO is 3.37 eV corresponding to 378 nm wavelength and distinctive electrooptical properties. The coherent blend of UV absorption with better transparency in the visible range makes it suitable candidate for optoelectronic devices that needed both the life expectancy and improved efficiency under working conditions [14, 15, 16, 17]. According to some recent papers [18, 19, 20], the effect of UV irradiation altered conductivity, surface morphology and structural properties of zinc oxide thin films significantly. C–Y. Tsay et al. reported two-fold improvement of photocurrent responsivity and a sharp increase in photocurrent under illumination with UVA light with Al doping in ZnO thin films [21]. Y.-K. Tseng reported that UV irradiation results in better crystallinity, solidity, and surface roughness. Their work also showed that, compared to non-UV treated samples, the films with UV irradiation results in good conductivity [22]. J. Kim et al. showed that the UV irradiation can improve structural properties significantly as well [23]. A. C. Marques et al. investigated the power output density of AZO thin films under UV light and found it to be increased during exposure of the films to UV-light, due to the photo-thermoelectric effect [24]. So, further investigation is required to access the quality of thin films after UV irradiation.

Here, Sol-gen spin coating was employed to produce thin films of Al doped ZnO (AZO) were prepared following non-alkoxide sol-gel spin

* Corresponding author.
E-mail address: mbillah@mme.buet.ac.bd (Md.M. Billah).

https://doi.org/10.1016/j.heliyon.2022.e08743
Received 27 July 2021; Received in revised form 20 November 2021; Accepted 7 January 2022

coating route and properties were examined thoroughly. Structural features were studied using Field Emission Scanning Electron Microscope (FE SEM) and X-ray Diffraction (XRD), optical properties using Ultraviolet-visible (UV-vis) spectroscopy and electrical properties using Four-Point probe. Dopant concentration yielding the best optical and electrical properties was optimized for future transparent conductors. Effects of extended period of UV irradiation have also been investigated.

2. Materials and methods

AZO thin films were deposited on a silica glass substrate. Precursor, solvent and stabilizer used are zinc acetate dehydrate ($Zn(CH_3COO)_2.2H_2O$), 2-methoxy ethanol (MOE) ($CH_3OCH_2CH_2OH$) and mono-ethanolamine (MEA) ($(OHCH_2CH_2)NH_2$) respectively. Aluminum nitrate nonahydrate ($Al(NO_3)_3.9H_2O$) was used as doping agent. MEA to zinc acetate molar ratio was 1.0. Concentration of metal ions in the solution was 0.4 mol/L. Dopant concentration was varied between 1.0 to 3.0 mol percent with respect to ZnO. To obtain a clear, homogeneous, and transparent solution, all of the elements were mixed in a stoichiometric ratio. The sol was stirred for 1 h at 80 °C. Solution was then aged. Ageing condition were room temperature and ageing time 24 h (RT). Dynamic spin coating was used to deposit thin films at a rotation speed of 1000 rpm for 10 s and 3000 rpm for 20 s. After each step, films were dried at 180 °C for 5 min. This procedure was repeated 3 times for 3 layers. Finally, at 500 °C the films were annealed for 2 h in furnace atmosphere. UV radiation was applied to the sample of highest conductivity prior to annealing at 500 °C. The UV source was a 100 W UV-A lamp (LH- 100/100-A, UV emission wavelength 365 nm) and the irradiation was performed by illuminating the sample by the UV source the in dark chamber.

Philips X-ray Diffractometer [PW 3040-X 'Pert PRO] was used for XRD pattern using CuK_α radiation, surface was observed using FE SEM: JEOL JSM 7600F and optical transmittance was recorded with UV–vis spectrometer [Halo DB -20/20s]. Bruker's Dektak XT Stylus Profiler was used for thickness measurement. Electrical resistivity and Hall coefficient were assessed using a Four-Point probe [LSR4; LCSMU-SW-TG1]. Apart from that, Surface roughness was measured using Mountains Lab Premium 9 Software from SEM micrographs.

3. Results and discussion

3.1. Effect of doping

3.1.1. Crystallographic structure

The hexagonal wurtzite structure of all the thin films were confirmed from the indexed XRD peaks (ICDD card no. 80-0075). No addition peak was observed for pure Al or Al_2O_3, or any other impurity phase which indicates the well diffusion of Al^{3+} in the crystal structure of ZnO (Figure 1). High degree of crystallinity of all the films are evident from the peak intensity and their sharp peak width.

Crystal size for all synthesized films were obtained using the Scherrer's Eq. (1),

$$D = 0.9\lambda/\beta cos\theta \quad (1)$$

where, D is crystal size, λ is CuK_α radiation wavelength of (0.15406 nm). Full width at half maximum (FWHM) β is measured in rad and θ is half of the Bragg diffraction angle.

With increasing Al concentration, a gradual decrease in major peak intensity was observed which indicates degradation of crystalline quality of ZnO resulted from the substitution of Zn^{2+} by Al^{3+} ions (Figure 2). Crystallite size was decreased by doping Al from 30.1 nm for pure ZnO to 27.1 nm for 3% AZO thin film as formation of Al–O–Zn in doped ZnO prevents crystal growth (Table 1). The increase in Bragg diffraction angle with increased doping concentration can be attributed to the presence of compressive stress generated by different lattice flaws [25, 26].

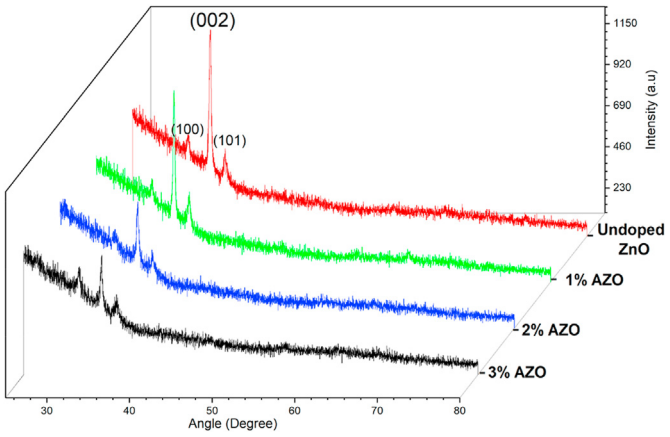

Figure 1. XRD of the thin films.

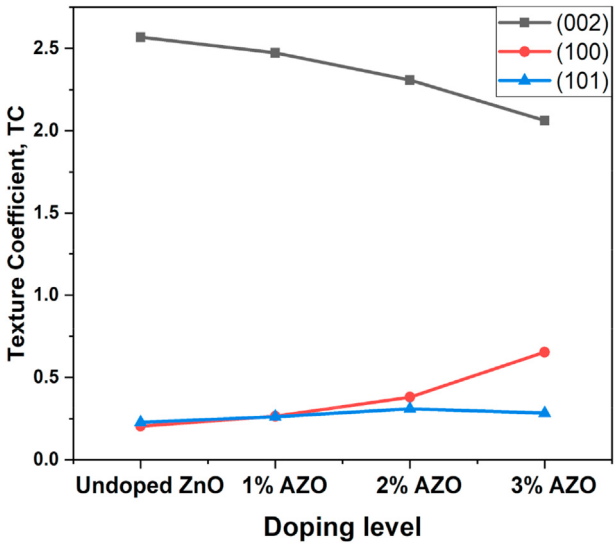

Figure 2. Effect of doping on texture coefficient.

The micro-strain was calculated using Williamson-Hall equation, Williamson Hall Plot is shown in Figure 3:

$$\beta\cos(\theta) = \frac{k\lambda}{D} + 4\varepsilon \ \sin(\theta) \quad (2)$$

here, β is FWHM, θ is half of the Bragg diffraction angle, D is mean crystallite size, ε is the micro-strain. Thus, a plot of βcos(θ) against 4sin(θ) is a straight line and slope of the plot represents average strain in the film.

The gradual increase of strain with increasing doping concentration due to variation in ion size of Al with Zn ions ($r_{Al}^{3+} = 0.054$ nm) and ($r_{Zn}^{2+} = 0.074$ nm) can be a reason for the deterioration in crystallinity on doping (Table 2) [27, 28]. Also, with excessive doping of 3 mol % Al, the greater

Table 1. XRD data assessment for the thin films.

Thin Films	2θ (degree) of (002) Peak	Average FWHM	Crystallite Size (nm)	Average Micro-strain
Undoped ZnO	34.3924	0.267	30.1	0.293
1 mol % Al doped ZnO (1% AZO)	34.4123	0.275	28.3	0.348
2 mol % Al doped ZnO (2% AZO)	34.4356	0.283	27.5	0.358
3 mol % Al doped ZnO (3% AZO)	34.4720	0.298	27.1	0.366

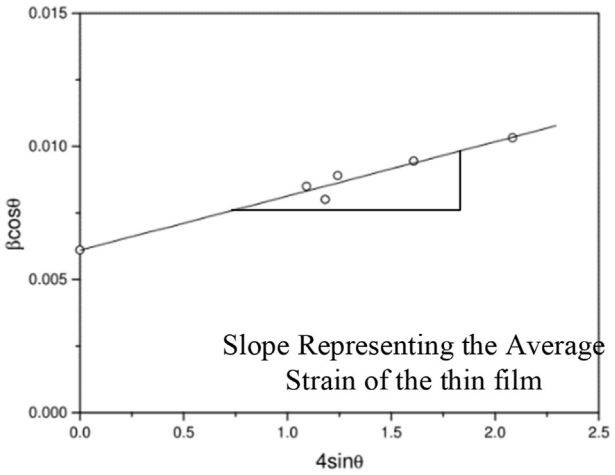

Figure 3. Williamson Hall Plot of AZO thin Films.

Table 2. Texture coefficient and film thickness for ZnO and AZO thin films.

Thin Films	Texture Coefficient, $TC_{(HKL)}$			Film Thickness (nm)
	(002)	(100)	(101)	393 nm
Undoped ZnO	2.56	0.20	0.22	287 nm
1 mol % Al doped ZnO (1% AZO)	2.47	0.26	0.26	250 nm
2 mol % Al doped ZnO (2% AZO)	2.30	0.38	0.31	227 nm
3 mol % Al doped ZnO (3% AZO)	2.06	0.65	0.28	225 nm

charge (+3) of aluminum can create more bonds with oxygen which degraded the quality of hexagonal wurtzite structure of Zinc oxide. Here, Al^{3+} substituted Zn^{2+} in the lattice. That means some zinc-oxygen bonds have been replaced by aluminum-oxygen bonds. Also, no phase of aluminum oxide was identified from XRD pattern. It seems that even if any small amount of aluminum oxide was formed, that was not significant and was below the detection limit of XRD.

Preferred orientation were calculated from the Harris's analysis [24] from texture coefficient as per Eq. (3)

$$TC_{(hkl)} = \frac{\frac{I_{(hkl)}}{I_{0(hkl)}}}{\frac{1}{N}\sum_{n=1}^{N}\frac{I_{(hkl)}}{I_{0(hkl)}}} \quad (3)$$

where, texture coefficient of plane (hkl) is $TC_{(hkl)}$; $I_{(hkl)}$ and $I_{0(hkl)}$ are the intensity of the planes of the thin films and randomly oriented ZnO powder respectively defined by (ICDD card no. 80-0075); N is diffraction peaks' number.

Texture co-efficient having values greater than one (unity) implies a greater degree of preferred orientation. As X-ray intensities depend on atomic structure factors, the deviation in the TC values from unity means change in atomic density along that plane [31]. The values of texture coefficient indicate preferred orientation along (002) plane for both undoped and doped films (Figure 2). The preferred orientation towards c axis gradually decreased with the increasing doping concentration. This indicates that the strong (002) orientation reduced with the substitution of Al in ZnO lattice. The greater values of TC to a particular plane corroborates with the increase in planer density along that plane [29, 30].

3.1.2. Optical properties

Figure 4 shows transmission and absorbance spectra in the wavelength range 300–1000 nm for undoped ZnO and AZO thin films prepared with various doping concentrations. Average transmittance of undoped ZnO was 86.28% and was dropped slightly for all the doped thin films. However, in the visible spectra, all films showed transparency greater than 80% and a sharp absorption edge in the 350–400 nm wavelength range, which can be credited to the intrinsic band gap of the films [31]. The rapid decline in transmittance near the fundamental absorption edge is the corroboration of the superior crystallinity of the films [5]. The superior crystalline nature with comparatively lower defect density makes it suitable candidate for optoelectronic devices [32, 33].

The estimation of direct band gap energy was obtained using the use of Tauc's law [34, 35].

$$(\alpha h\upsilon)^2 = C(h\upsilon - E_g) \quad (4)$$

Here, α is coefficient of optical bandgap, energy of incident photon is hν, C is a constant and E_g is optical band gap. By extrapolating the linear portion, the band gap values were estimated from the $(\alpha h\upsilon)^2$ vs E_g plots (Figure 3).

Band gap values on doping were higher than that for undoped ZnO (Figure 5). Band gap increased with increasing Al addition showing maximum band gap of 3.67 eV for 2% AZO. This increase can be attributed to the degenerate doping of Al. When Zinc oxide is doped with Al, the lowest band gets saturated with free electrons. Fermi level remains between conduction and valence bands for nominally doped semiconductors. However, Fermi level can is pushed into the conductive band minimum for degenerate doping, such as for Al. Therefore, the next available empty state now becomes the suitable candidate for higher unoccupied conduction state. This raises the lowest optical transition energy and the gap in the optical band. This phenomenon is known as the Moss-Burstein shift [36]. For further addition of Al above 2 mol %, bandgap was decreased. This decrease of E_g is believed due to the separation of excess Al atoms at grain limits as well as by the presence of the interstitial defect states [37]. This decrease also can be attributed to the exchange interactions between sp-d bands.

3.1.3. Film resistivity

Figure 6 depicts the difference in resistivity of undoped and AZO thin films with different doping concentrations. The resistivity was dropped

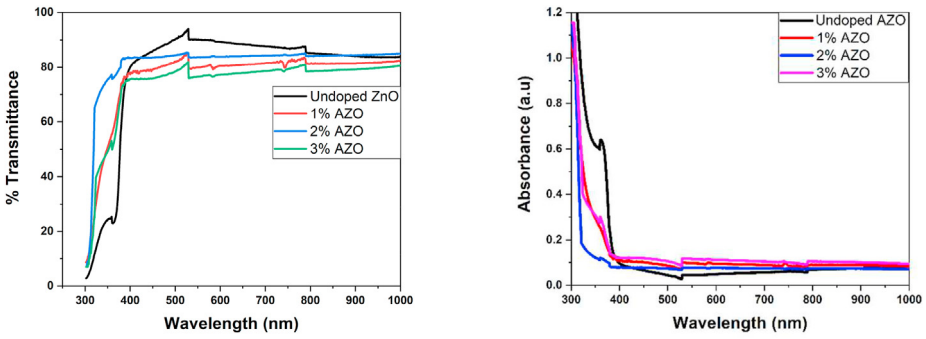

Figure 4. Optical transmittance spectra (left) and absorbance spectra (right) of ZnO and AZO thin films.

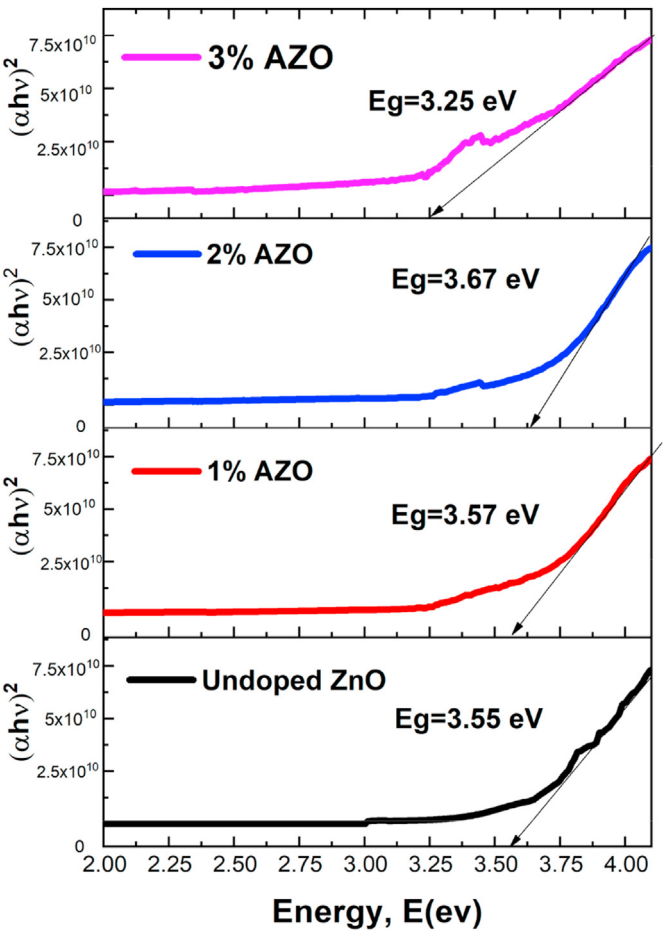

Figure 5. $(\alpha h\upsilon)^2$ vs E_g plot to calculate optical energy bandgap.

significantly with 1 mol % Al addition because of the excess carrier concentration resulted from Al doping and decreased further showing minimum resistivity of 2.05 Ω-cm for 2% AZO. Later, resistivity was increased with further Al addition. For such addition, carrier concentration decreases since increasing dopant might have formed impartial defects. Also these atoms do not provide free electrons. Decrease in crystallinity may also offset the effect of increased carrier concentration by decreasing carrier mobility leading to the declined conductivity for 3 mol percent doping [38].

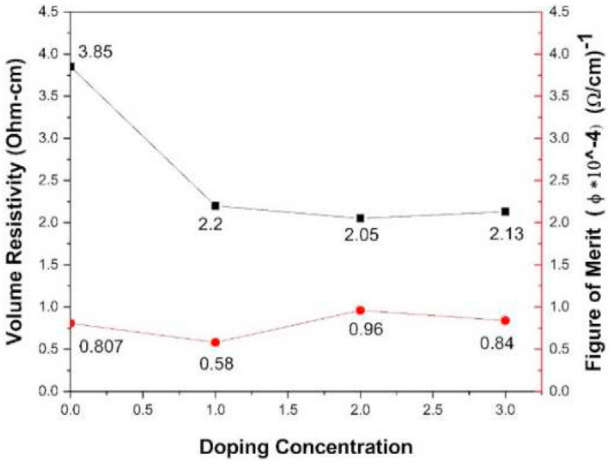

Figure 6. Volume resistivity and figure of merit with doping.

Table 3. Experimental results from XRD analysis of UV treated vs non-UV treated 2% AZO films.

Thin Films	2θ (degree) of (002) peak	Average FWHM	Crystallite Size (nm)	Average Micro Strain	Texture Coefficient $T_{(002)}$
2% AZO	34.4356	0.283	27.5	0.358	2.30
2% AZO UV-treated	34.4534	0.263	30.8	0.396	2.33

To quantify the optoelectronic properties, figure of merit (φ) was calculated using the following equation [39]-

$$\varphi = \frac{T^{10}}{\rho} \tag{5}$$

where, T is the transmittance value at 650 nm wavelength [40] and ρ is the volume resistivity. The maximum value of φ, best fusion of lower resistivity and higher transmission results in TCO films with comparatively better performance or quality [35]. The figure of merit was first decreased with initial addition of Al since the decrease in resistivity could not offset the decrease in transmittance compared to undoped ZnO. However, highest value of φ ($0.94 \times 10^{-4}\ \Omega^{-1}$-cm^{-1}) was obtained for 2% AZO film which is in well acceptable range for TCO to be used in optoelectronic applications [41, 42].

3.2. Effects OF UV irradiation

3.2.1. Crystallographic structure

The lengthy period of UV treatment has significant changes in crystal structure of 2% AZO thin film (Table 3). The average crystallite size increased with the UV treatment along with the increase in Texture coefficient along (002) plane. That indicates the tendency of the crystals to grow along (002) plane increased with prolonged UV treatment. UV treatment could also initiate the recrystallization of the grains causing rise in surface roughness of after irradiation which is evidenced in Table 4.

Average FWHM of (002) peak is reduced with the advent of UV treatment (Figure 7) and subsequently increase of the crystallite size was from 27.5 nm to 30.8 nm. The Braggs angle shifted towards higher values along with the increase in micro strain in the structure which suggest that the onset of UV treatment created compressive stress in the structure of AZO thin films [43, 44]. After the UV treatment, the increase in texture coefficient in (002) direction establishes the preferential c axis orientation of the crystals. So, the crystallographic properties improved in the (002) direction as the XRD peak intensity increased along with the decrease in FWHM values from 0.283 to 0.263. These results indicate that crystallinities towards c axis improved after prolonged UV treatment.

3.2.2. Optical properties

From the comparison of the transmission spectra for UV treated and non-UV treated 2% AZO thin films it is evident that absorption edge shifted to higher wavelength for the case of UV treated sample (Figure 8). This corresponds to the decreased optical band gap of 3.59 eV. This decrease in band gap with increasing crystallite size is well expected due to quantum confinement effect. The protracted UV exposure caused the increase in RMS surface roughness from 18.29 nm to 22.45 nm. 2 mol% AZO UV treated sample shows an average transmittance of 82.20% in visible region compared to 84.19% transparency in non-UV treated 2% AZO films which can be attributed to the increased RMS value and greater light scattering effect.

Upon reaching the visible spectra from UVA spectra there is a sudden increase in transparency in the thin film. This sudden change in transparency in UV region might be helpful in constructing various sensors

Table 4. Optical Properties summary of 2% AZO sample before and after UV treatment with reference to relevant references of Similar work.

Thin Films	Fraction of UV Light Blocked (%)	Average Transmittance in Visible Region (%)	Optical Bandgap (eV)	Conductivity (S/cm)	RMS Surface Roughness (nm)	References
2% AZO	33.35	84.19	3.67	0.3806	18.29 nm	Current Research
2% AZO UV- treated	42.49	82.70	3.59	1.177	22.45 nm	Current Research
Undoped ZnO	73	79.8	3.57	-	31 nm	[24]
2% Doped AZO	-	86	3.29	9.52	-	[27]
Undoped ZnO with 25 Hours UV treatment	40–45	85	3.24	-	13.23	[22]

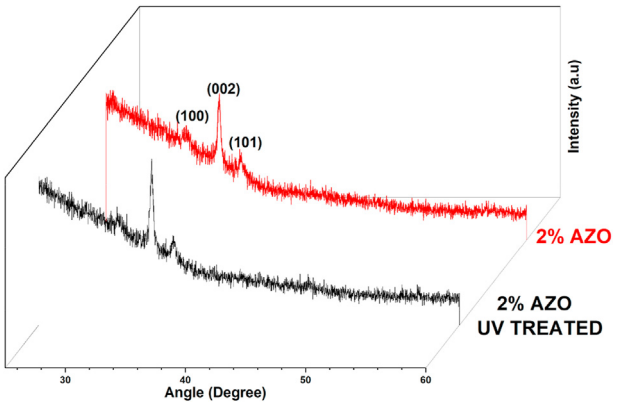

Figure 7. XRD patterns of films before and after UV treatment.

[45]. After UV treatment the 2% thin films showed greater capacity to block UVA radiation by 42.49% compared to non-UV treated samples which blocks by 33.35% as shown in Table 4. UV blocking capabilities of the thin films were calculated using Eq. (6). The overall light transmittance in each wavelength band is measured by the τ_{λ,λ_0} value, where λ and λ_0 is the range of the wavelength, which is evaluated, φ_{AM} 1.5 G (λ) is solar light intensity distribution function. Data was taken from National Renewable Energy Laboratory (NREL), weighted average is between 315 and 378 nm and $T(\lambda)$ is the weighted average of transparence in the 315 nm–378 nm wavelength for estimating UV blocking.

$$\tau_{\lambda,\lambda_0} = \frac{\int_{\lambda_0}^{\lambda} T(\lambda) \cdot \varphi_{AM1.5\ G}(\lambda).\, d\lambda}{\int_{\lambda_0}^{\lambda} \varphi_{AM1.5\ G}(\lambda).\, d\lambda} \text{X } 100 \quad (6)$$

3.2.3. Film resistivity

Prolonged UV irradiation caused noticeable improvement in the conduction of 2 % doped films (Table 4). UV exposure resulted in the enhanced conductivity. AZO thin films have a persistent photoconductivity because of activation due to light irradiation. UV irradiation for a long period affects excitation and activation of conduction band electrons and thus upgrades the electrical conductivity [46].

Hall coefficient were evaluated using Van Der Pauw method [47]. 2% AZO UV treated thin films have excess carrier concentration may be due to ionization of oxygen vacancies which work as donor sites in the AZO lattice. With the prolonged UV light absorption electron–hole sets are

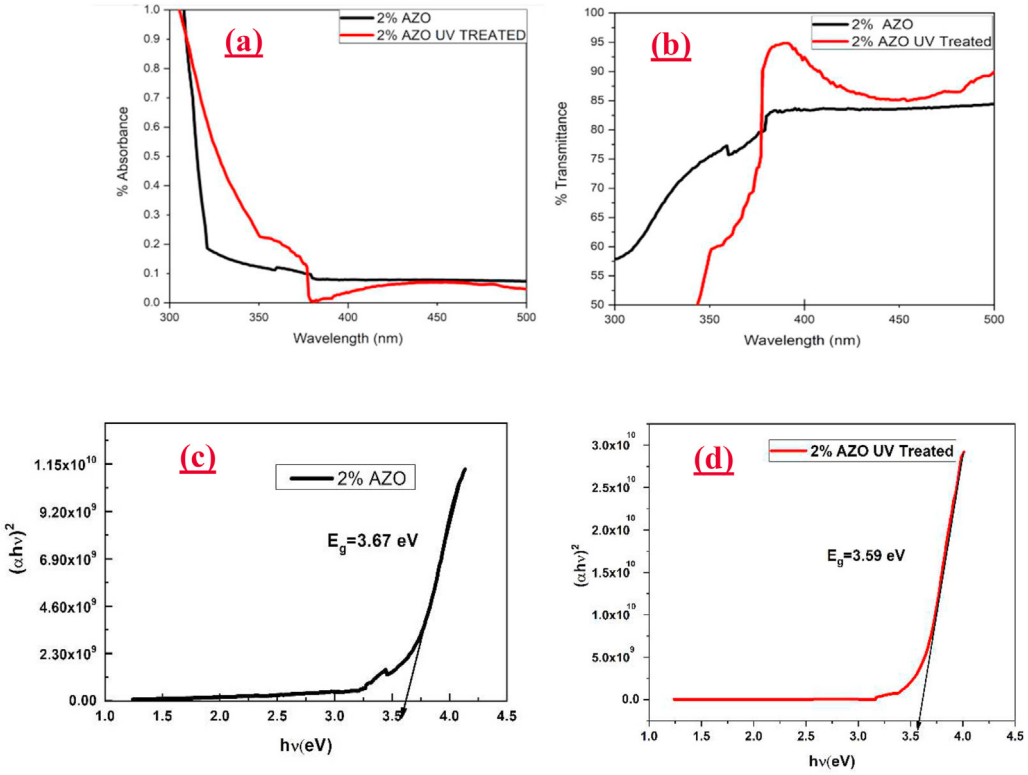

Figure 8. (a) Absorbance spectra, (b) transmittance spectra, band gap of (c) non-UV treated and (d) UV-treated 2% AZO.

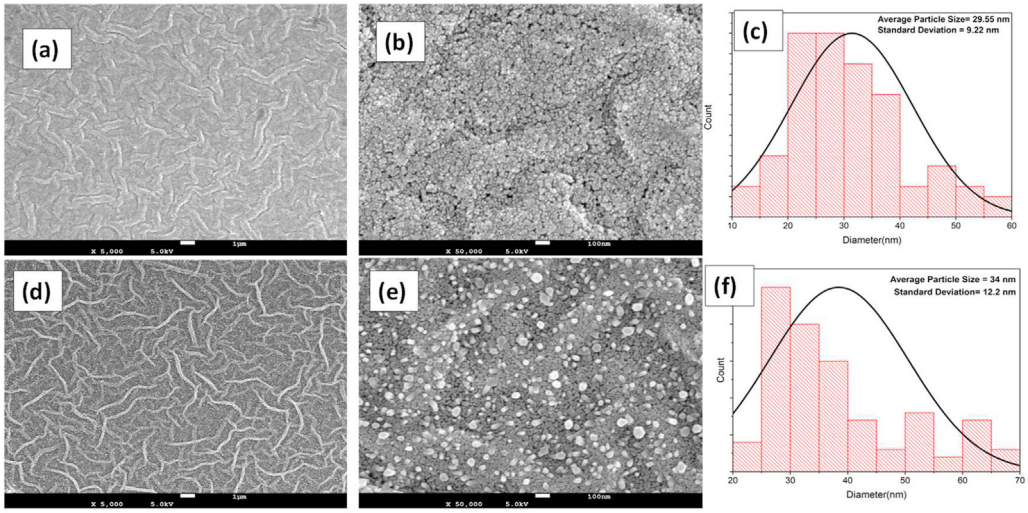

Figure 9. FESEM images and particle size distribution of (a, b, c) non-UV treated and (d, e, f) UV treated 2% AZO films.

created by UV light assimilation at beginning. Following hole diffusion to the grain boundaries, the chemisorbed species existing at these locations are oxidized, which might result in their desorption [48]. Because this process solely consumes holes, a buildup of electrons develops, leading to an growth in carrier density. As a result of the increased number of surface donors generated by UV irradiation, the electrical conductivity of the material is improved. Furthermore, it can decompose organic substances such as methoxy groups via photocatalytic reactions when exposed to UV light. These decompositions can result in photo-induced ion doping and the generation of free electrons on the 2% AZO UV treated thin film [49]. The availability of free elections may influence the increase in conductivity in UV-treated thin films.

3.2.4. Morphology of film surface

The micrographs demonstrated granular morphology of all the films with polycrystallinity in nature where each grain was formed due to multiple crystallite agglomeration (Figure 9). Ganglia-like patterns were found at low magnification for both pure ZnO and AZO thin films, which are typical of such films. The mentioned pattern development is driven by stress relief because of solvent evaporation during the drying process [40]. The average film thickness of the 2% AZO UV treated sample was 212 nm, while it was 237 nm for the non-UV treated sample. It validates the enhancing of the solvent evaporation process later on after it was put into UV chamber [50] and reduced the film thickness. Because the energy came from the UV light irradiation, it could move the molecules and could enhance the solvent evaporation process after putting it into UV chamber.

From the 3D images of the AZO samples in Figure 10 (b, d) it was detected that surface roughness intensified on UV treatment causing blockade of UV rays absorption into the sample which led to higher UV reflection.

4. Conclusion

In this study, all films were made following sol-gel spin coating and its properties were characterized afterwards. Varying concentration of Al,

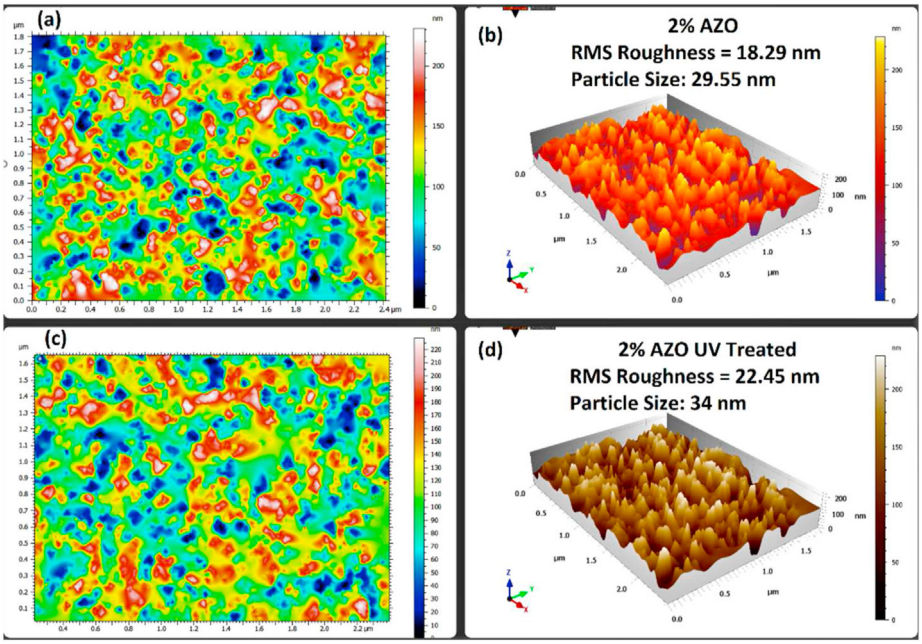

Figure 10. 2D and 3D images of (a, b) Non-UV Treated (c, d) UV treated 2% AZO films.

2% AZO annealed at 500 °C exhibited maximum optical band gap of 3.67 eV with a transmittivity of 84.19% and minimum volume resistivity of 2.05 Ω-cm. Low volume resistivity along with the high transmittance results in the high value of figure of merit for 2% AZO which makes it most suitable to be used in optoelectronic applications. The UV exposure on this doped AZO thin film showed a significant increase in conductivity with decreased band gap and better UVA protection capabilities under UV source. The UV irradiation shows significant change in RMS surface roughness and film thickness.

Declarations

Author contribution statement

Md. Irfan Khan, Tasratur Reaj Neha: Performed the experiments, analyzed and interpreted the data, wrote the paper.

Md. Muktadir Billah: Conceived and designed the experiments, analyzed and interpreted the data, contributed reagents, materials, analysis tools or data.

Funding statement

This research did not receive any specific grant from funding agencies in the public, commercial, or not-for-profit sectors.

Data availability statement

No data was used for the research described in the article.

Declaration of interests statement

The authors declare no conflict of interest.

Additional information

No additional information is available for this paper.

References

[1] H. Aydın, F. Yakuphanoglu, C. Aydın, Al-doped ZnO as a multifunctional nanomaterial: structural, morphological, optical and low-temperature gas sensing properties, J. Alloys Compd. 773 (Jan. 2019) 802–811.
[2] K.M. Sandeep, S. Bhat, S.M. Dharmaprakash, Structural, optical, and LED characteristics of ZnO and Al doped ZnO thin films, J. Phys. Chem. Solid. 104 (May 2017) 36–44.
[3] Y. Kim, W. Tai, Electrical and Optical Properties of Al-Doped ZnO Thin Films by Sol – Gel Process 253, 2007, pp. 4911–4916.
[4] T. Amakali, L.S. Daniel, V. Uahengo, N.Y. Dzade, N.H. de Leeuw, Structural and optical properties of ZnO thin films prepared by molecular precursor and sol–gel methods, Crystals 10 (2) (Feb. 2020). Art. no. 2.
[5] N. Srinatha, P. Raghu, H.M. Mahesh, B. Angadi, Spin-coated Al-doped ZnO thin films for optical applications: structural, micro-structural, optical and luminescence studies, J. Alloys Compd. 722 (Oct. 2017) 888–895.
[6] K.D.A. Kumar, S. Valanarasu, A. Kathalingam, V. Ganesh, Mohd. Shkir, S. AlFaify, Effect of solvents on sol–gel spin-coated nanostructured Al-doped ZnO thin films: a film for key optoelectronic applications, Appl. Phys. A 123 (12) (Nov. 2017) 801.
[7] Ü. Özgür, et al., A comprehensive review of ZnO materials and devices, J. Appl. Phys. 98 (4) (2005) 41301. Available:.
[8] P. Gondoni, et al., Structural and functional properties of Al:ZnO thin films grown by Pulsed Laser Deposition at room temperature, Thin Solid Films 520 (14) (May 2012) 4707–4711.
[9] A. Kuroyanagi, Properties of aluminum-doped ZnO thin films grown by electron beam evaporation, Jpn. J. Appl. Phys. 28 (2) (1989) 219–222.
[10] H.-C. Semmelhack, et al., Optical and electrical properties of epitaxial (Mg,Cd) xZn1−xO, ZnO, and ZnO:(Ga,Al) thin films on c-plane sapphire grown by pulsed laser deposition, Solid State Electron. 47 (12) (2003) 2205–2209.
[11] M.N.H. Mia, et al., Investigation of aluminum doping on structural and optical characteristics of sol–gel assisted spin-coated nano-structured zinc oxide thin films, Appl. Phys. A 126 (3) (Feb. 2020) 162.
[12] Z.Q. Xu, H. Deng, Y. Li, Q.H. Guo, Y.R. Li, Characteristics of Al-doped c-axis orientation ZnO thin films prepared by the sol–gel method, Mater. Res. Bull. 41 (2) (Feb. 2006) 354–358.
[13] J. Lee, K. Ko, B. Park, Electrical and optical properties of ZnO transparent conducting films by the sol–gel method, J. Cryst. Growth 247 (1-2) (2003) 119–125.
[14] O.S. Kushwaha, C.V. Avadhani, R.P. Singh, Preparation and characterization of self-photostabilizing UV-durable bionanocomposite membranes for outdoor applications, Carbohydr. Polym. 123 (Jun. 2015) 164–173.
[15] N. Rajagopalan, A.S. Khanna, Effect of size and morphology on UV-blocking property of nano ZnO in epoxy coating, Int. J. Scient. Res. Pub. (IJSRP) 3 (Issue 4) (April 2013).
[16] M. Eita, L. Wågberg, M. Muhammed, Spin-Assisted multilayers of poly(methyl methacrylate) and zinc oxide quantum dots for ultraviolet-blocking applications, ACS Appl. Mater. Interfaces 4 (6) (Jun. 2012) 2920–2925.
[17] A. Becheri, M. Dürr, P. Lo Nostro, P. Baglioni, Synthesis and characterization of zinc oxide nanoparticles: application to textiles as UV-absorbers, J. Nano Res. 10 (4) (Apr. 2008) 679–689.
[18] M. Sasani Ghamsari, S. Alamdari, W. Han, H.-H. Park, Impact of nanostructured thin ZnO film in ultraviolet protection, Int. J. Nanomed. 12 (2017) 207–216.
[19] C. Wang, et al., Surface morphology, electrochemical and electrical performances of ZnO thin films sensitized with Ag nanoparticles by UV irradiation, J. Mater. Sci. Mater. Electron. 30 (10) (May 2019) 9798–9805.
[20] W. Johansson, A. Peralta, B. Jonson, S. Anand, L. Österlund, S. Karlsson, Transparent TiO2 and ZnO thin films on glass for UV protection of PV modules, Front. Mater. 6 (2019).
[21] C.-Y. Tsay, W.-T. Hsu, Comparative studies on ultraviolet-light-derived photoresponse properties of ZnO, AZO, and GZO transparent semiconductor thin films, Materials 10 (12) (Dec. 2017). Art. no. 12.
[22] Y.-K. Tseng, F.-M. Pai, Y.-C. Chen, C.-H. Wu, "Effects of UV assistance on the properties of al-doped ZnO thin films deposited by sol-gel method," Electron, Mater. Lett. 9 (6) (Nov. 2013) 771–773.
[23] J. Kim, et al., Enhanced conductance properties of UV laser/RTA annealed Al-doped ZnO thin films, Ceram. Int. 43 (4) (Mar. 2017) 3900–3904.
[24] A.C. Marques, et al., Stability under humidity, UV-light and bending of AZO films deposited by ALD on Kapton, Sci. Rep. 9 (1) (Nov. 2019) 17919.
[25] M. Ohring, Materials Science of Thin Films, second ed., Academic Press, 2001.
[26] B.D. Cullity, S.R. Stock, Elements of X-Ray Diffraction, third ed., Pearson, Upper Saddle River, NJ, 2001.
[27] M.-C. Jun, J.-H. Koh, Optical and structural properties of Al-doped ZnO thin films by sol gel process, J. Nanosci. Nanotechnol. 13 (5) (May 2013) 3403–3407.
[28] G.B. Harris, X. Quantitative measurement of preferred orientation in rolled uranium bars, London, Edinburgh, Dublin Philosoph. Magaz. J. Sci. 43 (336) (Jan. 1952) 113–123.
[29] R. Bhardwaj, Amardeep Bharti, J. Singh, K. Chae, N. Goyal, S. Gautam, Structural and electronic investigation of ZnO nanostructures synthesized under different environments, Heliyon 4 (2018).
[30] M.H. Mamat, M.Z. Sahdan, Z. Khusaimi, A.Z. Ahmed, S. Abdullah, M. Rusop, Influence of doping concentrations on the aluminum doped zinc oxide thin films properties for ultraviolet photoconductive sensor applications, Opt. Mater. 32 (6) (Apr. 2010) 696–699.
[31] N. Jabena Begum, R. Mohan, K. Ravichandran, Effect of solvent volume on the physical properties of aluminium doped nanocrystalline zinc oxide thin films deposited using a simplified spray pyrolysis technique, Superlattice. Microst. 53 (2013) 89–98.
[32] H. Shen, H. Zhang, L. Lu, F. Jiang, C. Yang, Preparation and properties of AZO thin films on different substrates, Prog. Nat. Sci.: Mater. Int. 20 (Nov. 2010) 44–48.
[33] K. Ravichandran, et al., Impact of spray Flux Density and Vacuum Annealing on the Transparent Conducting Properties of Doubly Doped (Sn + F) Zinc Oxide Films Deposited Using a Simplified spray Technique, 2014.
[34] D. Navas, A. Ibañez, I. González, J. Palma, P. Dreyse, Controlled dispersion of ZnO nanoparticles produced by basic precipitation in solvothermal processes, Heliyon 6 (2020), e05821.
[35] N.I. Rasli, H. Basri, Z. Haru, Zinc oxide from aloe vera extract: two-level factorial screening of biosynthesis parameters, Heliyon 6 (1) (2020), e03156 [32] I Hamberg, C G Gramquist, J App Phys 60 (1986) R123.
[36] H. Dondapati, K. Santiago, A.K. Pradhan, Influence of growth temperature on electrical, optical, and plasmonic properties of aluminum:zinc oxide films grown by radio frequency magnetron sputtering, J. Appl. Phys. 114 (14) (2013).
[37] A. Babar, P. Deshamukh, R. Deokate, D. Haranath, C. Bhosale, K. Rajpure, Gallium doping in transparent conductive ZnO thin films prepared by chemical spray pyrolysis, J. Phys. Appl. Phys. 41 (13) (2008) 135404. Available:.
[38] B. Sarma, D. Barman, B.K. Sarma, AZO (Al:ZnO) thin films with high figure of merit as stable indium free transparent conducting oxide, Appl. Surf. Sci. 479 (Jun. 2019) 786–795.
[39] S.A. Knickerbocker, A.K. Kulkarni, Calculation of the figure of merit for indium tin oxide films based on basic theory, J. Vac. Sci. Technol. 13 (3) (May 1995) 1048–1052.
[40] J. Qin, et al., Ultrahigh figure-of-merit in metal–insulator–metal magnetoplasmonic sensors using low loss magneto-optical oxide thin films, ACS Photonics 4 (6) (Jun. 2017) 1403–1412.
[41] N. Tarwal, et al., Photoluminescence of zinc oxide nanopowder synthesized by a combustion method, Powder Technol. 208 (1) (2011) 185–188.
[42] D. Guo, K. Satob, S. Hibinob, T. Takeuchi, H. Bessho, K. Kato, Low-temperature preparation of (002)-oriented ZnO thin films by sol–gel method, Thin Solid Films 550 (2014) 250–258.
[43] A.T. Vai, V.L. Kuznetsov, J.R. Dilworth, P.P. Edwards, UV-induced improvement in ZnO thin film conductivity: a new in situ approach, J. Mater. Chem. C Mater. Opt. Electron. Dev. (2014) 1–10, 00.

[44] J.S. Edinger, et al., Highly transparent and conductive indium-doped zinc oxide films deposited at low substrate temperature by spray pyrolysis from water-based solutions, J. Mater. Sci. 52 (14) (Jul. 2017) 8591–8602.
[45] E.M. Mkawi, K. Ibrahim, M.K.M. Ali, M.A. Farrukh, A.S. Mohamed, The effect of dopant concentration on properties of transparent conducting Al-doped ZnO thin films for efficient Cu2ZnSnS4 thin-film solar cells prepared by electrodeposition method, Appl. Nanosci. 5 (8) (Nov. 2015) 993–1001.
[46] J. Nomoto, H. Makino, T. Yamamoto, High-Hall-Mobility Al-doped ZnO films having textured polycrystalline structure with a well-defined (0001) orientation, Nanoscale Res. Lett. 11 (1) (Jun. 2016) 320.
[47] J. Hong, H. Wagata, K. Katsumata, K. Okada, N. Matsushita, Effects of thermal treatment on crystallographic and electrical properties of transparent conductive ZnO films deposited by spin-spray method, Jpn. J. Appl. Phys. 52 (11R) (Oct. 2013) 110108.
[48] Y. Shapira, R.B. McQuistan, D. Lichtman, Relationship between photodesorption and surface conductivity in ZnO, Phys. Rev. B 15 (4) (Feb. 1977) 2163–2169.
[49] Z. Cao, Z. Zhang, F. Wang, G. Wang, Synthesis and UV shielding properties of zinc oxide ultrafine particles modified with silica and trimethyl siloxane, Colloids Surf. A Physicochem. Eng. Asp. 340 (2009) 161–167.
[50] C.-C. Lee, M.-C. Liu, M. Kaneko, K. Nakahira, Y. Takano, Influence of thermal annealing and ultraviolet light irradiation on LaF3 thin films at 193 nm, Appl. Opt. 44 (32) (Nov. 2005) 6921–6926.